Climatology of the middle atmosphere temperature from long-term lidar measurements at mid- and low-latitudes.

I. Stuart McDermid [a], Thierry Leblanc [a], Philippe Keckhut [b], Alain Hauchecorne [b], C. Y. She [c], and David A. Krueger [c]

[a] ~~JPL~~ Jet Propulsion Laboratory, California Institute of Technology, Table Mountain Facility, Wrightwood, CA 92397

[b] Service d'Aéronomie du CNRS, 91371 Verrières-le-Buisson, France

[c] Department of Physics, Colorado State University, Fort Collins, CO 80523

ABSTRACT

Long term measurements from several lidar instruments, located at 44.0°N, 40.6°N, 34.4°N, and 19.5°N, were used to develop a new climatology of the middle atmosphere temperature. For each instrument, the measurements on every day of the year over the entire record were averaged to build a composite year of temperature profiles. The lidar climatologies were compared to the CIRA-86 model which appears to be systematically too cold between 90 and 95 km, by ≥20 K, and possibly 6-8 K too warm around 80 km, making its use as a reference questionable at these altitudes. The annual and semi-annual components of the seasonal variability and the 2- to 33-day period variability were also investigated. An annual cycle with 6-7 K amplitude in the upper stratosphere, increasing to 15-20 K at 80 km, is observed at mid-latitudes. At lower latitudes, a semiannual oscillation (SAO) propagates downward from 85 to 30 km and is characterized by a stronger first cycle than the second (4 K and 2 K amplitude). The 2- to 33-day variability at mid-latitudes shows a maximum during winter around 40 km and in the mesosphere. Finally, sudden seasonal transitions, highly consistent between all instruments, have been observed, in particular in the early winter mid-latitudes with a two-step warming of the mesosphere between 65 and 85 km.

Keywords: lidar, temperature, climatology, stratosphere, mesosphere, mesopause, middle atmosphere, SAO.

1. INTRODUCTION

The temperature structure of the middle atmosphere has been studied for several decades. The first investigations used rocketsondes and falling spheres to measure temperature profiles up to 60–90 km but with relatively poor accuracy. Later, the first systematic temperature profiles derived from Rayleigh lidar measurements of the relative density of the middle atmosphere provided improved vertical resolution and accuracy [1]. Currently, lidar measurements provide the best vertical resolution and accuracy for middle atmosphere temperature studies (stratosphere and mesosphere, ~15 to ~110 km). Also, they can provide long-term data series relatively absent of instrumental drift and an integration of the measurements over several hours removes most of the gravity wave-like short scale disturbances. Therefore they are among the most suitable instruments for looking at local variations of the middle atmosphere temperature over a wide spectrum of time scales. This paper describes a seasonal climatology of the middle atmosphere temperature derived from lidar measurements obtained at several mid- and low-latitude locations. Results from the following lidars, which have all obtained a long- or at least mid-term measurements record, were used in this study: the two Rayleigh lidars of the Service d'Aéronomie du CNRS, France, located at the Observatoire de Haute Provence (OHP, 44.0°N) and at the Centre d'Essais des Landes (CEL, 44.0°N), the two Rayleigh lidars of the NASA-Jet Propulsion Laboratory, USA, located at Table Mountain, California (TMF, 34.4°N) and at Mauna Loa, Hawaii (MLO, 19.5°N), and the Colorado State University, USA, sodium lidar located at Fort Collins, Colorado (CSU, 40.6°N). The overall data set extends from 1978 to 1997 with different periods of measurements depending on the instrument. Three of the instruments are located at primary or complementary stations (OHP, TMF, MLO) within the Network for Detection of Stratospheric Change (NDSC).

2. THE INSTRUMENTS, DATABASE AND DATA PROCESSING

At mid-latitudes the CNRS-SA Rayleigh lidar at OHP (44.0°N, 6.0°E) has obtained measurements between 30 and 95 km from 1978 to the present with 75 to 300 m vertical resolution, and that at CEL (44.0°N, 1.0°W) from 1986 to 1994 with 300 m vertical resolution. Profiles are obtained during the entire night if the weather conditions are good (no cloud and weak wind). This gives an average of 5-6 hours integration of nighttime measurements about 4-5 days a week (150-200 profiles per

year). The total estimated temperature error at the top of each profile is about 20-25 K including a priori initialization and statistical noise. This error drops to less than 1 K at mid-range (typically 55 km) and below [2,3]. The CSU (40.6°N, 105.1°W) Na lidar has obtained mesospheric temperature measurements in the Na layer between 80 and 110 km since 1989 with an initial 75 m vertical resolution smoothed over 3 km [4]. Quality, regular nighttime temperature measurements, i.e., on average four to five nights a month with 4 hours or more observations each night, were started in May 1991. Observation on nights with good winter weather conditions occasionally lasted longer than 11 hr and statistically the observations were evenly distributed throughout the night. The total estimated temperature error is less than 4 K and 8 K at the top and bottom of the profiles respectively, dropping to 0.6 K at mid-range (typically 90 km).

At lower latitudes, the NASA-JPL Rayleigh lidars located at TMF (34.4°N, 117.7°W) and MLO (44.0°N, 155.6°W) have obtained temperature measurements between 30 and 80 km since 1988, and between 15 and 90 km since 1993 respectively [5]. Most of the routine measurements comprise a 1.5-2.0 hour integration experiment, usually at the beginning of the night 4-5 nights a week, insuring a good survey of stratospheric ozone and temperature as required by the NDSC program. The associated temperature errors are similar to those of the French Rayleigh lidars but the top of the profiles are slightly lowered [3]. To avoid any confusion of definitions, MLO will be considered hereinafter as a "tropical" latitude site and TMF as a "sub-tropical" latitude site in contrast with the other sites located at "mid-latitude".

For all instruments, each individual temperature profile was interpolated to obtain data points every one kilometer thus making the data analysis and the comparisons between instruments easier. For the OHP and TMF instruments with a long period of measurements the earlier years were not used. There are two main reasons for not using the entire database. 1) For OHP there were only a limited number of measurements during the years 1978-1983 so that omitting these years does not lose much information. Also, it is interesting to compare the current climatology (1984 - 1995) with that previously obtained for the period 1978-1989 [6]. 2) For both OHP and TMF the results obtained during the first months or years of measurements and certainly before processing to an operational routine mode were considered experimental or preliminary and may have been affected by instrumental changes, and/or by some noisy profiles. This is not the case for MLO since the lidar group in charge with this instrument is the same as for the TMF instrument (NASA-JPL). For the Rayleigh instruments the top of the profiles was truncated about 10 km lower than the initial cut-off altitudes cited above. This way, the results containing a non-negligible part of a priori information and/or noise are not be shown and the resulting statistical error drops by at least a factor 3. This error is still high (~ 5 K) for an individual profile but the long period and/or the large number of measurements for most of the instruments will reduce it to few kelvins for the composite daily and monthly mean profiles. High confidence levels are expected up to 75 km altitude. Also, the bottom of the TMF profiles was truncated at 32 km instead of 30 km to avoid any direct effect of volcanic aerosols, especially after the eruption of Pinatubo (eruption in June 1991, major effect in spring-summer 1992). For the CSU sodium instrument, depending on the photon noise, typical measurement accuracies for the nightly mean temperatures are ~0.6 K near the peak (92 km) and ~ 4 to 8 K at the edges (80 km and 108 km) of the Na layer. Thus, unlike Rayleigh and Raman scattering whose accuracy decreases as altitude increases, the sodium lidar measurement is most accurate near 92 km where the sodium density peaks. Although temperature measurements were typically made between 80 and 110 km at Fort Collins, Colorado, the hours of observation and altitude ranges covered are shorter in summer due respectively to shorter nights and lower Na densities compared to winter. Therefore, only CSU profiles between 84 and 105 km are used for this climatological study. At OHP, CEL, TMF and MLO, the effect of the Pinatubo eruption (June 1991) was observed in the profiles below ~30 km. The total number of profiles obtained per month is highly variable, depending on the instrument.

3. DATA ANALYSIS AND RESULTS

3.1 Climatological temperatures

For each instrument, all individual temperature profiles, from 249 to 1244 profiles depending on the instrument, were merged into a composite single year of data. A weighted running average with a triangular 33-day width filtering scheme was applied to each day of the composite year that a profile was available. The remaining days with no profile were filled with an interpolated profile obtained using a two-dimensional minimum curvature spline surface method. Although these interpolated profiles were plotted they were not retained in the numerical database in order to avoid inaccuracies in the different analysis steps described in this section. No removal of tidal structures was performed. At mid-latitudes the semidiurnal tide is expected to be dominant with a few kelvins amplitude at 80 km. For OHP, CEL, and CSU, most of the measurements were taken over the entire night minimizing the effect of the 12-hour oscillation. At TMF, where measurements are performed only during 2 hours in the routine mode, the top the profiles is lowered to 75 km and both the diurnal and semidiurnal amplitudes have decreased significantly [7]. At MLO the role of the diurnal and semidiurnal tides may not be negligible above 80 km and similarly for the diurnal component at CSU above 90 km. The mean annual temperature climatologies obtained for OHP, CEL, CSU, TMF, and MLO are presented in figure 1.

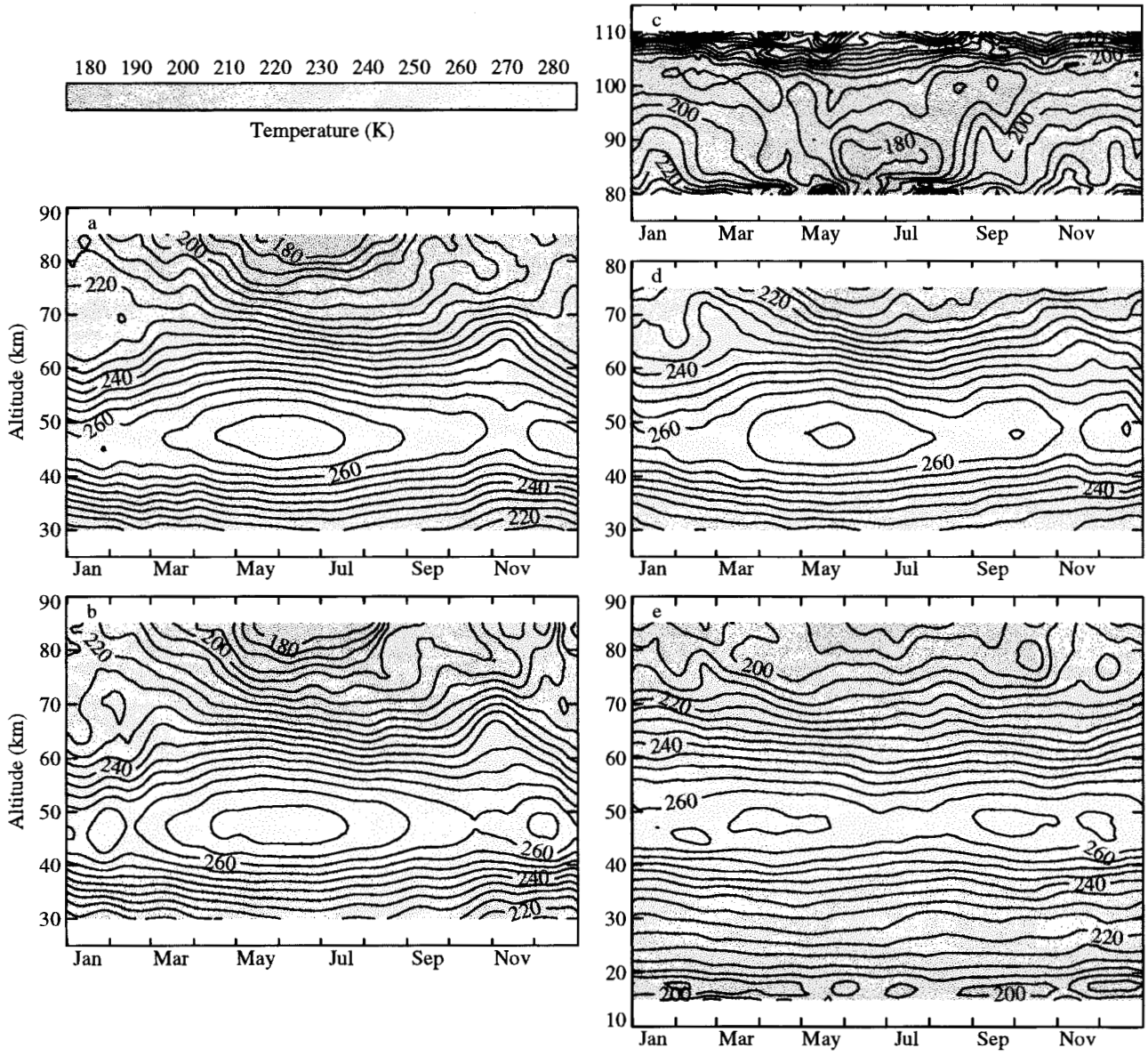

Figure 1. Climatological temperatures obtained from lidar measurements at (a) OHP (44.0°N, 6.0°E), (b) CEL (44.0°N, 1.0°W), (c) CSU (40.5°N, 105.1°W), (d) TMF (34.4°N, 117.7°W), and (e) MLO (19.5°N, 155.6°W).

For OHP, CEL and TMF (Fig. 1(a)(b)(d)) a familiar mid- and subtropical-latitude warm summer and cool winter stratosphere is observed with a maximum of 272 K in May-June and a minimum of 255 K in early November at the stratopause altitude of 47 km. A characteristic warm winter/cold summer mesosphere is also observed with a maximum of 220 K in December and January, and a minimum of 195-200 K in May-June at 75 km. For OHP, temperatures lower than 175 K are observed at 85 km in June-July which is in good agreement with previous climatologies [6] and 2-5 K colder than the 175-180 K measured by the Na lidar at Fort Collins, Fig. 1(c). The weak negative vertical temperature gradient observed in winter at OHP, CEL and TMF is the consequence of the seasonal average of the so-called mesospheric temperature inversions occurring during the entire winter at OHP and CEL, and more specifically in February at TMF. The temperature pattern above CSU is not very different from that described in a previous climatology [8]. The main difference is in spring and fall where the so-called double temperature minimum is no longer a significant part of the climatology. Instead, a continuously cooling layer in spring and a warming layer in fall can be observed between 85 and 95 km. As for the temperature inversions, this can be interpreted as the result of the seasonal averaging, i.e. the filtering. The double minimum is now only observable in early April. The most significant feature observed in figure 1(c) is the evidence of a 2-level mesopause [8]. The winter mesopause is characterized by a minimum of 195 K located about 103 km, and 2 absolute minima (185-190 K) in spring and fall. The summer mesopause is

characterized by extremely cold temperatures (< 180 K), minimum at 85 km. The transition between the summer and winter mesopause is short, taking less than two months (April-May and August-September) as already reported [9]. This double mesopause has also been observed at polar latitudes [10] with winter mesopause temperatures of 190-195 K at Andenes, Norway (69°N), and a rapid transition in August between the summer mesopause located at 82 km and the winter mesopause located at 98 km.

Another remarkable similarity between OHP, CEL, CSU and previous observations at Urbana (40°N, 88°W) [11] is the total temperature difference of 40 K between winter and summer in the 85-95 km range. Despite the high variability reported at these altitudes (Bills and Gardner reported a 115 K maximum amplitude at 90 km) the calculated climatological temperatures are 210 K, 215 K and 220 K, in winter, and 170 K, 175 K and 180 K, in summer, at Urbana, OHP, and CSU respectively.

Figure 1(e) (MLO) clearly shows a semiannual cycle at the stratopause, maximum temperature 266 K at 47 km, and an annual cycle in the lower stratosphere with a very cold minimum of 190 K at 17 km identified as the tropical tropopause. As expected at these latitudes, the amplitude of the seasonal variations is weak. At the top (80-85 km), where the effect of the mesospheric tides is the largest, the measured cold temperatures are more representative of early night temperatures than nightly (or even a 24-hour) mean temperatures.

Since the results obtained at OHP and CEL are almost identical, data from both sites have been computed and plotted together as a single mid-latitude site (44°N) hereinafter called "OHP+CEL". Results from OHP and CEL will be shown separately only if significant differences are observed or if there is a need for an inter-comparison.

3.2 Difference from CIRA-86

The monthly mean lidar temperatures were subtracted from the monthly mean CIRA-86 temperatures [12]. The temperature difference between the observed lidar climatology and the CIRA-86 climatology is plotted in Figure 2 (a) (OHP+CEL and CSU), (b) (TMF) and (c) (MLO). For convenience, and since they have quasi-separated altitude ranges, OHP+CEL and CSU are presented on the same plot, Fig. 2(a), with a separating altitude of 84-85 km.

The differences between the CIRA-86 model and the lidar observations have two primary origins. The first is the small magnitude of the CIRA temperature variability compared to the observed temperatures. In our case this applies at mid-latitudes in the stratosphere, and in the mesosphere. This is partly due to the poor vertical and horizontal resolutions causing extensive smoothing when computing the CIRA temperatures and partly due to residual noise and/or variability when computing the temperatures observed by lidar. This source of error is also related to transient processes such as sudden seasonal transitions from summer to winter or stratospheric warmings. The CIRA temperatures have a 1-month time resolution and cannot accurately take into account processes with time scales of one month or less. The associated errors are generally large. For OHP+CEL observed temperatures are up to 10 K colder than CIRA in December and January below 40 km. This can be explained by the out-of-phase occurrence, between late January and February, of stratospheric warmings at OHP and CEL and its equivalent occurring earlier in the CIRA model (December-January). Consequently the CIRA is too warm in December and January. In the lower mesosphere OHP+CEL and TMF temperatures are warmer than the CIRA. A maximum departure of 10 K around 70 km is observed in February at TMF, 4 K at 60 km in April-May for all mid-latitudes sites, and 4 K (respectively 8 K) at 60-70 km in November above OHP/CEL (respectively TMF). In the middle mesosphere OHP/CEL temperatures are colder than CIRA with a maximum departure of 10 K in November at 75-80 km.

The second reason for the differences is related to a systematic error in the CIRA temperatures which is also due to its poor or irregular horizontal resolution and poor vertical resolution, or due to drifting measurements. This error remains small in the middle atmosphere but is not negligible since it can affect an entire layer or season. For OHP and CEL (bottom of Fig. 2(a)) the observed temperatures are systematically 2-4 K colder than the CIRA between 30 and 40 km, especially in summer, and 2-6 K colder between 70 and 80 km, while no systematic error is observed at stratopause altitudes. These results are similar to those obtained previously over an earlier period [6]. For TMF, Fig. 2(b), no significant departure of this type is observed. For MLO, Fig. 2(c), the entire region between 15 and 55 km is colder than the CIRA (up to 4 K in the upper stratosphere) which is in good agreement with the Solar Mesospheric Explorer (SME) / CIRA-86 comparisons at similar latitudes [13]. At mesopause altitudes this error is remarkably large at mid-latitudes as illustrated by the difference CSU-CIRA (top of Fig. 2(a)) where a very large positive departure, >16 K, is observed in the entire mesopause region (90-95 km). Once again, similar SME/CIRA-86 departures have been reported [13] suggesting that the CIRA is definitely too cold at these heights and latitudes. Consequently, the lidar temperature initialization using CIRA might lead to too cold temperatures at the top of the OHP and CEL profiles. This polluting effect of the priori information led CNRS/SA and JPL to investigate the use of Na lidar or satellite (SME, UARS) climatological data for initializing the top of their Rayleigh temperature profiles.

At MLO, Fig. 2(c), the temperature departures are smaller than at mid- and subtropical-latitudes. This is not surprising since the variability is itself smaller at low-latitudes. Consequently the errors due to the annual and semi-annual amplitudes, and

due to the seasonal transitions are minimized. In the entire middle atmosphere, except at two times of the year between 60 and 70 km, the CIRA model is warmer.

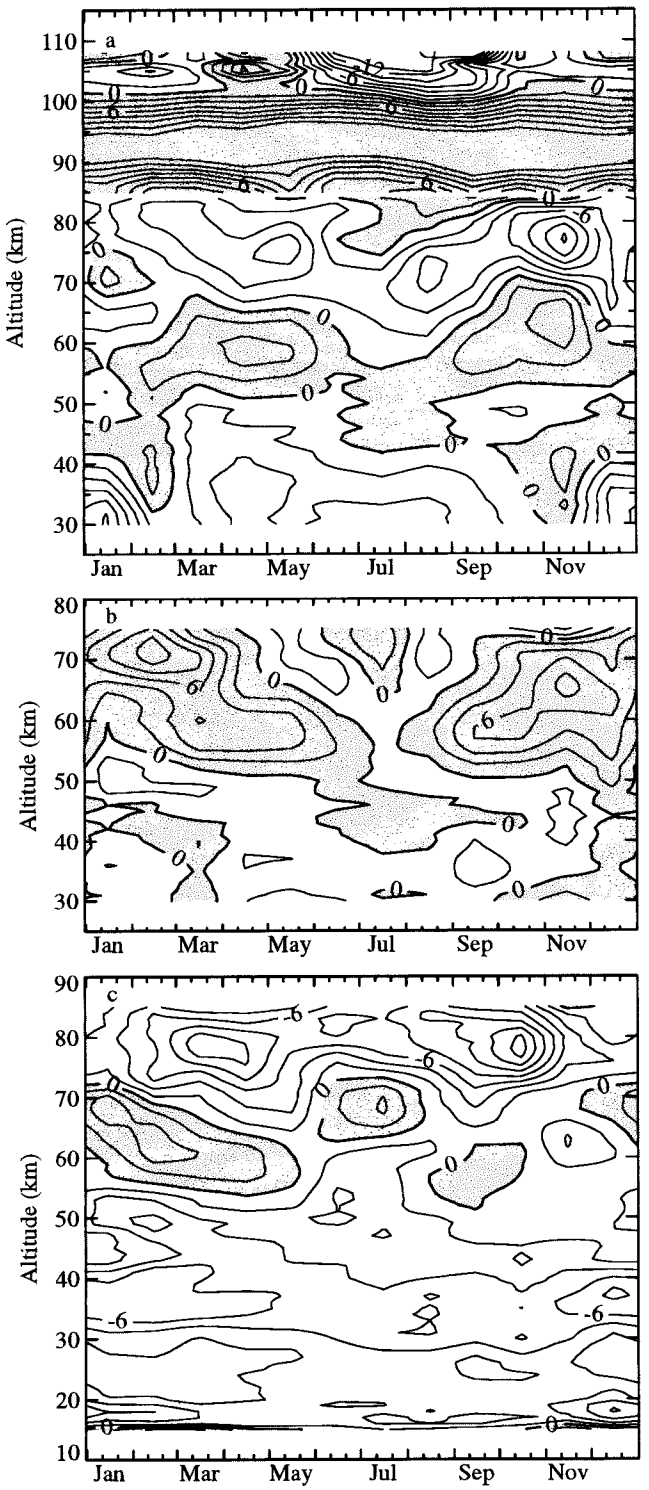

Figure 2. Monthly mean differences from the CIRA-86 temperatures: (a) OHP+CEL and CSU, (b) TMF, (c) MLO.

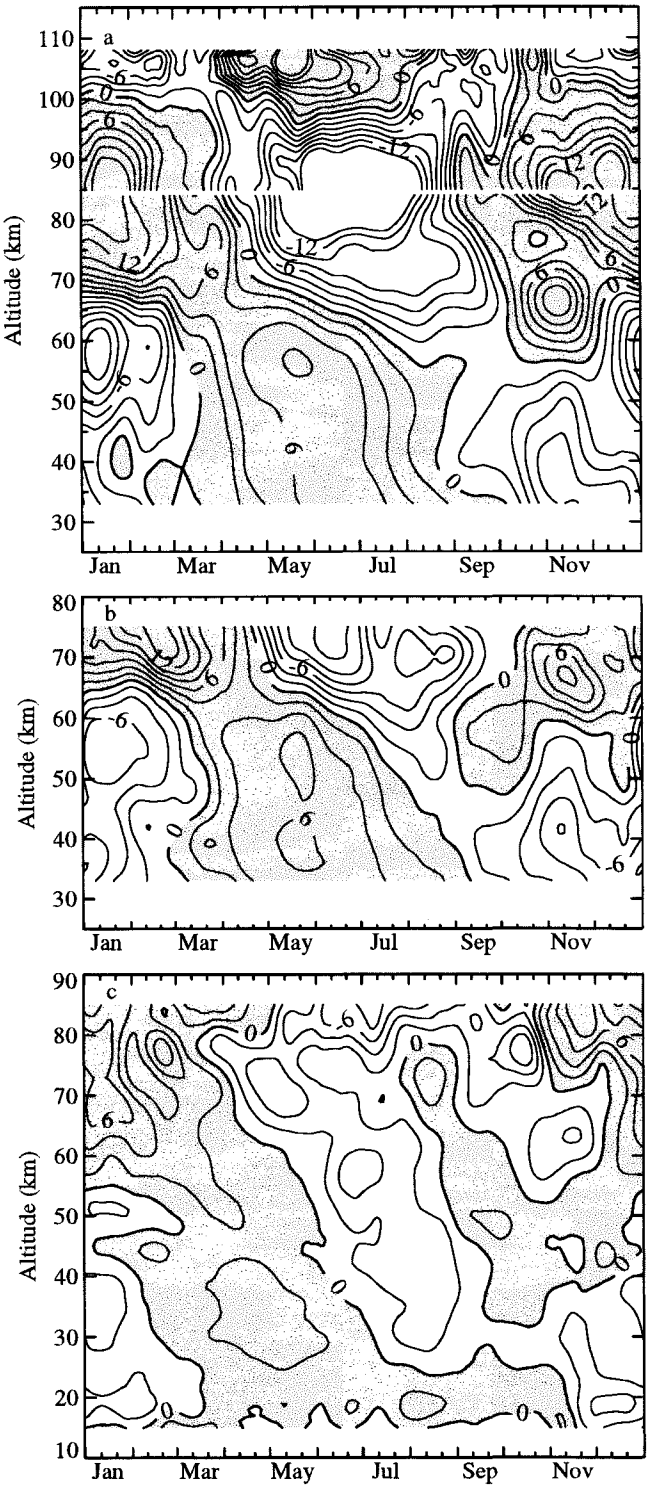

Figure 3. Daily mean deviation from the annual mean temperature: (a) CSU and OHP+CEL, (b) TMF, (c) MLO.

In the stratosphere the systematic departure is about 2 K. At 80 km a maximum negative departure of 10 K can be observed. In the 60-70 km region CIRA is colder as already observed at mid-latitudes (Fig. 2(a)(b)) and reported at all latitudes by SME [13]. Also, a very special pattern is observed at the beginning of the year. A negative departure is propagating downward from 80 km associated with a positive departure around 65 km and another negative departure between 50 and 55 km. The similarity in the downward propagation for these three different layers suggests a possible wavelike structure. In fact, the associated vertical wavelength is close to that of the diurnal tide (28 km for the first mode) suggesting that the temperatures measured by lidar at MLO are representative of early night temperatures. If so, the downward propagation observed in figure 2(c) might be a consequence of the seasonal variation of the tidal phase. A non-negligible role of the Semiannual Oscillation (SAO) may also account for such a structure. A longer database at MLO is in any case necessary to provide a more detailed explanation. Whatever the source of departure between the lidar observations and the CIRA-86 model it has to be noted that these departures are in very good qualitative agreement with those previously reported [13]. Quantitatively, some differences of few kelvins remain but this can easily be explained by the different vertical resolutions of the SME and lidar instruments and by a non-negligible interannual variability.

3.3 Temperature deviations from the annual mean

The annual mean temperature profile was then subtracted from each available daily composite profile to obtain the daily deviation from the annual mean. Figure 3 represents this deviation for (a) CSU and OHP+CEL, (b) TMF, and (c) MLO. As expected for CSU, OHP+CEL, and TMF, Fig. 3(a) and (b), an annual cycle is clearly dominant in both the stratosphere and mesosphere. At 67-70 km its phase compared with the solar flux is inverted, leading to the classic warm summer stratosphere and cold summer mesosphere and vice-versa in winter. A second phase inversion is clearly observed at CSU (top of Fig. 3(a)) around 95-100 km, marking the transition between the dynamically and chemically or radiatively driven upper mesosphere. These plots, in particular figure 3(a), also show a warm late-winter centered at 35-40 km. This is the signature of the stratospheric warmings occurring from January to March at mid- and high-latitudes. This signature is still observable in figure 3(b) but with a weaker magnitude. Another warm spot is observed at 65-67 km in November reaching 11 K for OHP/CEL and 8 K for TMF. This feature can also be observed in figure 1(a)(b)(d) as a bulge of warm temperatures in November between 60 and 70 km.

In contrast to the mid-latitudes sites, MLO (Fig. 3(c)) primarily exhibits a semi-annual cycle between 25 and 80 km altitude. This is not surprising since MLO is located at 19.5°N and is influenced by the equatorial dynamical pattern which in turn is affected by both northern and southern hemispheres. The semi-annual cycle observed here is almost a continuous downward propagating oscillation with an approximate vertical speed of 12 km/month and can be identified as the thermal semi-annual oscillation (SAO). The so-called mesopause and stratopause SAOs appear here as a combined single SAO propagating downward from the mesopause to 30 km with minimum amplitude at 45 km. A phase inversion is observed near 82 km similar to that observed by SME at 83 km [14]. The oscillation is strongly modulated with the first cycle being stronger than the second. The seasonal asymmetry of the wind and temperature SAO has been widely reported (see for example a recent wind and temperature SAO climatology [15]). However, due to the relatively northward location of MLO, the late winter maxima and early summer minima of the mid-latitude annual cycle and the equatorial SAO are in phase and may also cause the first oscillation of the semi-annual cycle to be of larger magnitude than the second. Also observed in figure 3(c) is an annual cycle at 20-km and below, more likely related to upper tropospheric variability and troposphere-stratosphere interaction.

3.4. Annual and semiannual cycles

The annual and semiannual components can be separated by fitting the results to a multi-parameter sinusoidal function of the form:

$$T(t,z) = T_0(z) + T_1(z)\cos\left[\frac{2\pi(t-\varphi_1(z))}{365 \text{ days}}\right] + T_2(z)\cos\left[\frac{2\pi(t-\varphi_2(z))}{182.5 \text{ days}}\right] \quad (1)$$

where T_1 and φ_1 (respectively T_2 and φ_2) are the amplitude (K) and phase (days) of the annual (respectively semiannual) cycle and T_0 is the annual mean temperature (K) at altitude z. The amplitudes and phases of the annual and semi-annual cycles are plotted for all sites in figure 4. The agreement between OHP, CEL, TMF and CSU is remarkable for both the amplitude and phase of the annual and semiannual cycles. They confirm the previous calculations [6] and also the observed 4 K smaller annual amplitude around 82-86 km at CSU than at OHP and CEL [16]. The annual cycle at these sites exhibits several maxima, of 7 K, 20 K, and 13 K located respectively at 35, 80 and 105 km, and minima located at 62 km for TMF, 65 km for OHP, and CEL, and 99 km for CSU. The minima correspond, as shown in figure 4(c), to the phase inversion between the stratosphere and the mesosphere (62-65 km) and between the mesosphere and thermosphere (~100 km), giving rise to the dominance of a dynamically driven mesosphere. The main difference between TMF and the mid-latitude sites is found in the amplitude

between 50 and 60 km where the TMF amplitude is smaller than for OHP and CEL. Another significant difference is the altitude of the phase inversion which is about 4 kilometers lower than at OHP and CEL. This is consistent with the results shown in figure 3. In these figures the most significant fraction of the mid-latitude annual cycle occurs during the first six months. During these first six months the amplitude of the TMF warm cycle has its minimum in early April at 61 km while for OHP and CEL it has its minimum at 64-65 km. In terms of phase, between 55 and 70 km the TMF warm cycle propagates downward one month earlier than that at OHP and CEL which correspond to a 4 km difference shown in figure 4(a)(c).

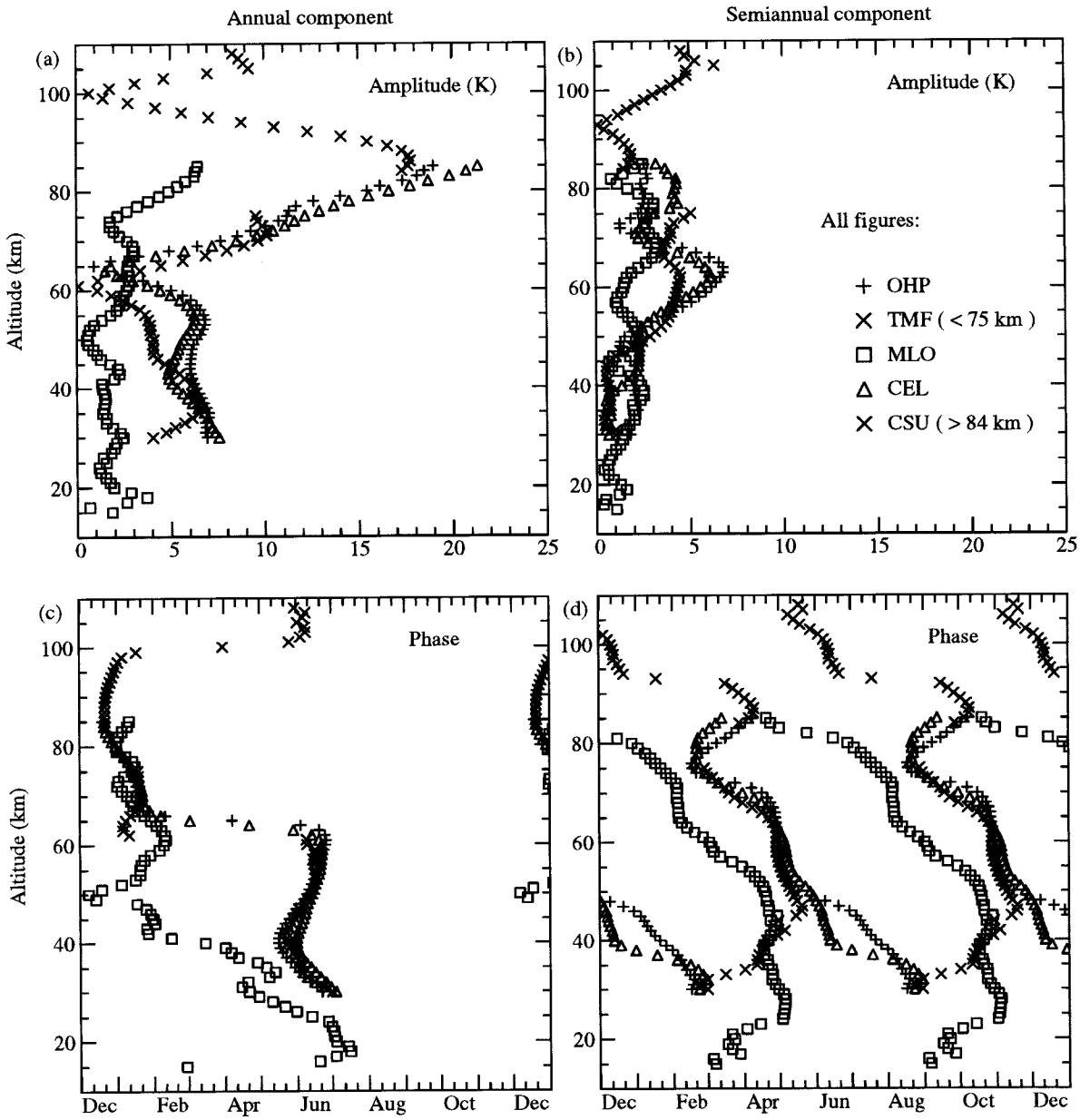

Figure 4. Amplitudes (top) and phases (bottom) of the annual (left) and semiannual (right) cycles observed at OHP (triangles), TMF (X), MLO (squares), CEL (crosses), and CSU (X)

The shift in phase observed at TMF is due to the influence of the early first cycle of the low-latitude semi-annual oscillation observed at MLO in figures 3(c) and 4. For all mid-latitude sites the semiannual component is weaker than the annual component except at the altitudes of annual phase inversion where it reaches a maximum of 5-7 K at 60-64 km for TMF, OHP, and CEL, and 6 K at 105 km for CSU. As observed in figure 3(a)(b), the maximum at 60-64 km is due to the warm spot occurring in early November at almost the same altitude as that of the node in the annual amplitude (3 K) occurring in early April. The maximum at 104±2 km points out the interplay between the dynamically and chemically driven mesosphere

and can be explained using the CSU temperature field in figure 1(c). In June the very cold summer mesopause is located around 85 km and the temperature between 100-105 km is mostly influenced by a radiatively warm lower thermosphere. In winter the mesopause is located much higher, in the 100-105 km region, and its warmer temperatures are dynamically driven. Between summertime and wintertime, i.e. near the equinoxes, the 100-105 km region is influenced by both the cold summer mesopause and by the fact that the mesopause level has risen from 85 to 100 km. The resultant temperatures at that time of the year are colder than in summer and winter leading to a strong apparent semiannual component.

3.5 2- to 30-day temperature variability

Having established the climatological average it is now interesting to look at the temperature variability on shorter time scales. Since most of the initial profiles were integrated over several hours, or even over a night, a large part of the variability due to gravity waves has already been removed. Thus, if the standard deviation of each daily composite profile from a 33-day averaged profile is calculated an indicator of the wave activity of all atmospheric waves with periods between typically 2 and 33 days can be obtained. These include most of inertio-gravity waves and planetary waves. In contrast to OHP, CEL and CSU, where most of the gravity waves with periods shorter than 24 hours are removed, periods between 4 and 24 hours may sometimes be included for TMF and MLO. The running standard deviation from the 33-day average at the altitude z for a given day d will be defined as:

$$\sigma_T(z,d) = \sqrt{\overline{\left(T(z,d) - \overline{T}(z,d)\right)^2}} \quad \text{where } \overline{X}(z,d) = \frac{1}{n_d} \sum_{d'=d-16}^{d'=d+16} X(z,d').\delta_{d'} \text{ denotes the 33-day running average of the quantity X,}$$

$\delta_{d'}$ denotes the Dirac function for the day d' (0 if no data taken this day, 1 if data were taken), and n_d denotes the total number of days within the 33-day window for which data were taken, all years included.

The variance due to the instrumental noise associated with the lidar measurements should be small enough compared to the variance associated with the waves if we want to extract a significant geophysical signature. However, this is not the case in the upper part of the profiles. For this reason the variance of the instrumental noise must be subtracted from the calculated standard deviation σ_T. For the Rayleigh instruments the growth rate of the standard deviation due to instrumental noise is related to the atmospheric scale height since the statistical error is a function of the photon counts, i.e. the atmospheric density [1]. The variance due to instrumental noise was computed with the assumption of a 10 K statistical error at the altitude of 93 km exponentially decreasing downward, with a 7 km mean atmospheric scale height:

$$\sigma_n(z,d) = 10 * \exp\left(\frac{z\text{-}93\,\text{km}}{7\,\text{km}}\right) \qquad \text{for all sites except CSU}$$

For CSU, the statistical noise is related to the Sodium layer density and minimum at its center (~92 km). Since we do not show CSU data below 86 km, the variance due to instrumental noise has been computed with the assumption of a 10 K statistical error at the altitude of 112 km exponentially decreasing downward, with a 7 km mean atmospheric scale height, and with no effect below the maximum sodium density:

$$\sigma_n(z,d) = 10 * \exp\left(\frac{z\text{-}112\,\text{km}}{7\,\text{km}}\right) \qquad \text{for CSU}$$

The filtered standard deviations ($\sigma_f = \sigma_T - \sigma_n$) are plotted in figure 5 for (a) OHP+CEL and CSU, (b) TMF, and (c) MLO.

Although not optimized, this simple filter will remove most of the variance due to instrumental noise in the upper part of the profiles without removing the geophysical information. By comparing all 3 figures, it is clear that the variability with periods between 2 and 33 days has its maximum at mid-latitudes and decreases significantly towards the tropical latitudes. Despite the different methods of vertical filtering and the different integration periods of each instrument, the qualitative and quantitative agreement and consistency are remarkable. As expected, and as previously shown [6], the maximum wave activity at mid-latitudes occurs in winter. In the stratosphere, a winter maximum of 10-12 K occurs between 35 and 45 km at OHP/CEL (Fig. 5(a)), (50% smaller at TMF, Fig. 5(b)). This maximum is principally associated with stratospheric warmings but are also certainly associated with all other inertio-gravity and planetary wave activity. After the observed maximum of 10 K around 40 km and a minimum of 8 K at 55 km, a second winter maximum of 12 K is observed in the mesosphere at CSU and OHP+CEL (50% smaller at TMF) between 70 km and 95 km. Then a second minimum occurs around 100 km. The mesospheric maximum is associated with the mesospheric temperature inversions whose amplitude can frequently reach 40 K, with a 1- to 5-day averaged duration [17]. However, due to the basic filter applied here to remove the instrumental noise it is not clear where the mesospheric maximum actually occurs and what is its true magnitude. The most important result is that

OHP and CSU are in very good agreement again, even quantitatively (Fig. 5(a)), and that a maximum of variability is observed around 75 km associated with the mesospheric temperature inversions.

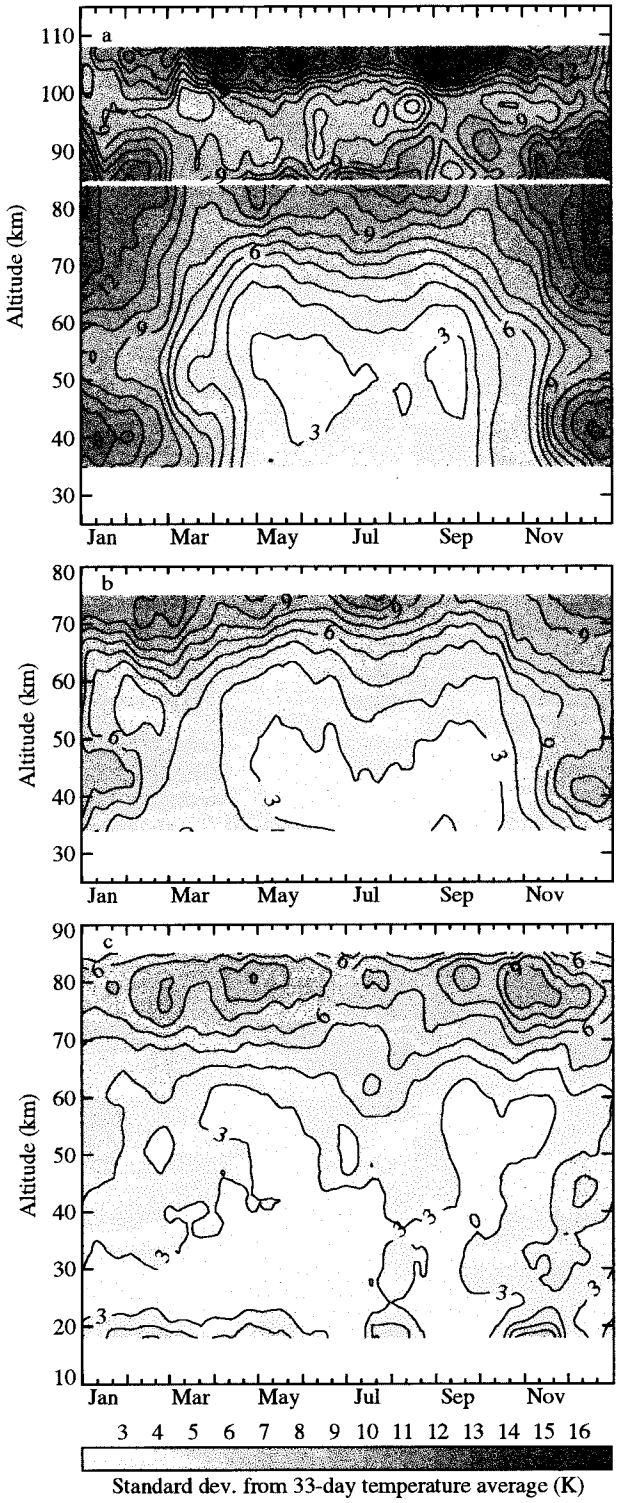

Figure 5. Daily mean standard deviation from the 33-day averaged temperature (K) at (a) OHP+CEL and CSU, (b) TMF and (c) MLO.

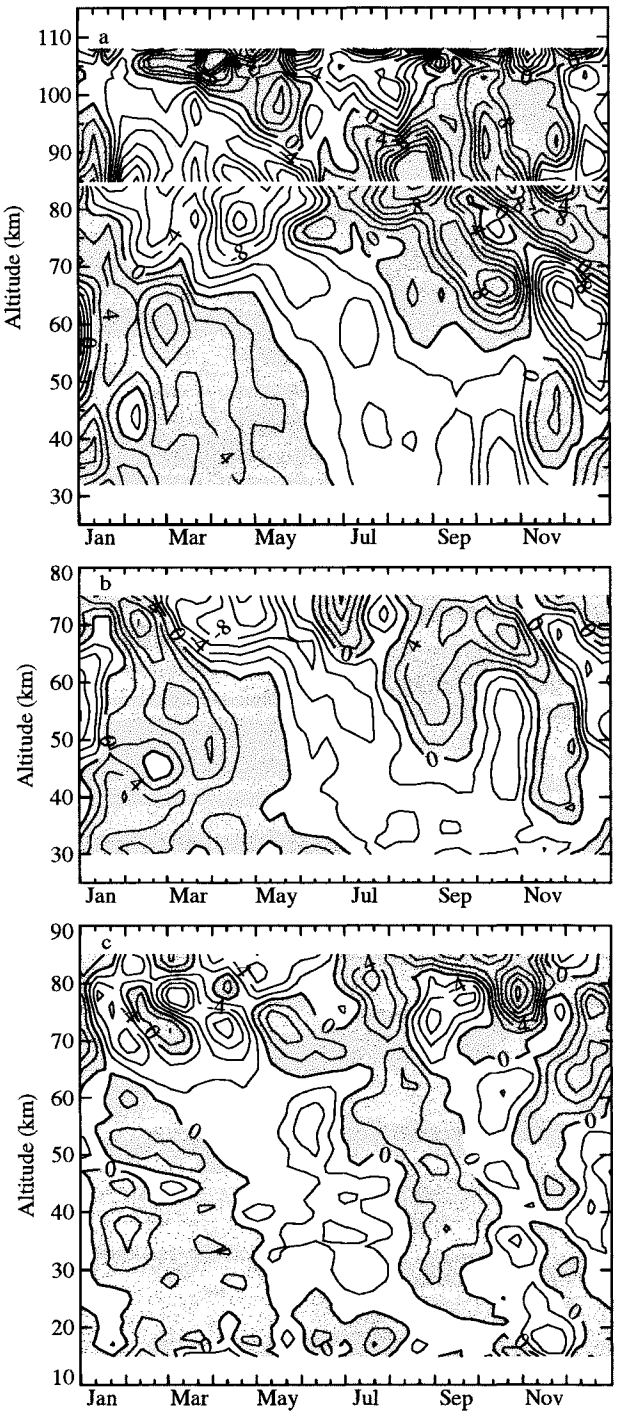

Figure 6. Time variation of the climatological temperatures (K/month) given in figure 1 for (a) OHP+CEL and CSU, (b) TMF, and (c) MLO.

In summer the standard deviation is very low, even at mid-latitudes, confirming the weak wave activity during this season at these latitudes. Two secondary maxima are nevertheless observed in early May and early September around 80 km at OHP, while late March and late September appear to be the quietest periods of the year. At MLO, figure 5(c), the extratropical planetary waves are too far away to account for the temperature variability, except in the upper stratosphere in December. Greater activity is also observed in the lower stratosphere showing the high variability of the tropical tropopause. In the mesosphere two maxima are observed following a remarkably symmetrical pattern with a six month interval. First reaching 8 K before the equinoxes, they then reach 10 K in early May and November at 83 km.

3.6 Seasonal evolution of the temperature

In order to characterize the seasonal temperature variations the temporal evolution of the temperature, i.e. the time derivative, was calculated:

$$T'(t,z)=\frac{\delta T}{\delta t}=\frac{T(t+1,z)-T(t-1,z)}{d(t+1,z)-d(t-1,z)} \tag{2}$$

where $d(t)$ and $d(t+1)$ are two consecutive days of measurement (not necessarily two consecutive dates). The results are presented in figure 6. As for the previous Figures, CSU and OHP+CEL are plotted together, with the OHP+CEL data at 84 km and below and the CSU data at 85 km and above. The profiles are plotted with a 10-day time resolution and are smoothed over 3 points so that the information appears here as quasi-monthly mean values allowing a better comparison with CIRA. Once again, the agreement between OHP+CEL and CSU is remarkable.

At mesospheric and stratospheric mid- and subtropical-latitudes (Fig. 6(a)(b)) the summertime temperature variations are quite small below 75 km with a maximum cooling rate of 4 K/month below 75 km while the wintertime evolution is much more chaotic. Above 75 km the entire year looks chaotic with cooling rates greater than ±8 K/month. Non-negligible instrumental noise may contribute to the larger variability at these altitudes. However, it is clear that the summer upper mesosphere cools down in two steps. The first step is in February around 85 km, with a maximum cooling rate of 12 K/month, and the second step is in late April around 75 km and above. All mid-latitudes instruments (i.e. OHP, CEL, CSU and TMF) agree in this respect. Then, a first strong heating period takes place in late August (>14 K/month as shown in figure 6(a). This mesospheric warming propagates downward with a maximum of 10 K/month at 65 km in mid-October. Immediately after this warming period a short quiet period follows extending from September around 85 km to late October at 70 km. Then a second strong warming period occurs with a maximum of 10 K/month at 90 km in October propagating downward with a maximum of 6 K/month in early November. Then, from late November to late December the temperature behavior in the mesosphere is driven by the occurrence of the mesospheric temperature inversions. A large cooling (up to –14 K/month) is observed around 65 km and a moderate warming (+7 K/month) is observed at 75 km. In the stratosphere the winter cooling occurs in a regular manner in October (-4 to -8 K/month) in the entire 30-55 km layer.

For MLO, figure 6(c), the semiannual oscillation is characterized by weak warming rates (maximum 4 K/month at 38 and 45 km in January and August respectively) and cooling rates (~2 K/month) in the entire middle atmosphere except the upper mesosphere. Above 75 km stronger values (up to 15 K/month) are observed randomly distributed in time. Once again, a possible explanation is the effect of the mesospheric tides. At these altitudes, the amplitude of the diurnal and semidiurnal tides can reach 5-10 K. However, the different times of measurements do not vary critically (typically, all measurements are obtained within the first 5 hours of the night). Some other effects related to insufficient statistics and/or residual noise have to be taken into account. A longer database may lead to significant insights in the future.

For TMF, figure 6(b), an expected intermediary scheme between OHP+CEL and MLO is observed. The mid-latitude annual cycle is dominant but with some modulation due to the influence of the lower latitudes. For example, the early winter cooling of the stratosphere occurs at the same time as for OHP+CEL (late October) and the summer cooling in the mesosphere behaves like at OHP+CEL. The first strong winter mesospheric warming, shown on figure 6(a), is also observed for TMF but with weaker amplitude (+8 K/month at 67 km). However, the winter mesosphere behaves quite differently. The strong cooling period occurring from November to December between 55 and 65 km at OHP+CEL now occurs in late December to early January nearer to 55 km altitude. In addition, the strong warming period observed at OHP at 75 km is no longer observed in December but in February and at 70 km. The lower latitudes seem to affect significantly the temperature behavior at TMF during this period. The 4 K/month cooling rate in mid-October at 60 km observed at MLO is in opposite phase with the 10 K/month warming rate observed at 65 km at OHP. The consequence is a moderate warming rate of 4 K/month at TMF. Also, a 6 K/month warming rate observed at MLO at 65 km in early December is in opposite phase with the large 14 K/month cooling rate observed at OHP, resulting in a moderate 6 K/month cooling rate at TMF.

4. DISCUSSION AND CONCLUSION.

When studied all together, figures 1 to 6, and especially figure 6, give important new insights in the middle atmosphere temperature climatology. Most of the differences from the CIRA-86 climatology can be explained as can most of the differences observed between some instruments. As has been observed in all previous middle atmospheric temperature climatologies [6,13-16], a dominant annual cycle is observed at mid-latitudes and a semiannual cycle is dominant at lower latitudes. Below 60 km the annual cycle is in phase with the solar flux leading to a warm summer and cold winter stratosphere and lower mesosphere, as expected. Between 65 and 100 km, the annual cycle is in opposite phase to the solar flux, as a consequence of a dynamically driven mesosphere, and is characterized by a warm winter and cold summer mesosphere. Above 102 km thermospheric processes lead again to an annual cycle that is in phase with the solar flux. The observed downward propagating temperature behavior in the mesosphere points out the dominant wave driven pattern, in contrast with the vertically stationary behavior observed below 50-55 km. At MLO the dominant semi-annual cycle is modulated by the northern mid-latitude annual cycle thus contributing, together with the well known seasonally asymmetric equatorial SAO, to the first warm-cold cycle (winter and spring) being stronger than the second (summer and fall).

The 2-33 day variability shown in this climatology is also in good agreement with that shown in a previous climatology [6]. A maximum in the planetary wave activity is observed in winter in the stratosphere and the maximum variability is also observed in the winter mesosphere due to the occurrence of the temperature inversions. An important latitudinal gradient is also observed with decreasing variability from the mid- to the lower-latitudes.

Systematic departures from the CIRA-86 model were observed which confirms the similar results of previous comparisons [6,13]. In particular, too cold temperatures in the CIRA-86 model lead to a large difference (> 15 K) around 90-95 km compared to lidar results, possibly due to an overestimation of non-LTE effects in the computation of the CIRA-86 temperatures [18]. On an annual basis CIRA-86 seems to be too warm around 55-60 km, too cold between 60 and 75 km, too warm between 75 and 85 km, and much too cold around 90-95 km. Above 100 km the high temperature variability caused by thermospheric processes leads to a large negative departure of 16 K in summer. Consequently, between 95 and 105 km the vertical gradient of the temperature difference CSU-CIRA is extremely steep in summer, reaching –3.4 K/km (see top of Fig. 2(a)), illustrating the poor accuracy of the CIRA-86 model in this region. Using too cold CIRA-86 temperatures at 90-95 km for initialization can lead to some dramatic temperature errors at the very top of the Rayleigh lidar profiles. For this reason the CNRS/SA and JPL lidar groups are currently investigating the use of a different a priori temperature information to avoid such uncertainty.

When the seasonal variation of temperature at mid-latitudes is studied in more detail some new interesting results are obtained. Instead of steady cooling in spring and steady warming in fall in the mesosphere (as predicted by the vertically and temporally smoothed CIRA-86 model) some short periods of strong cooling and warming are observed. It appears that the cooling of the summer mesosphere is characterized by two short periods of strong cooling occurring in late January at 85 km and in April-May between 80 and 85 km. The warming of the winter mesosphere occurs suddenly in late August at 85 km and then propagates slowly downward, reaching altitudes of 65-70 km in October. A second warming period occurs at 85 km in October. In the lower and middle mesosphere (55-80 km) a dramatic event disturbs the well-defined mid-latitude winter mesosphere warming. In late November and December a strong cooling period occurs around 60-65 km together with a weak warming period at 75 km, more than two months after the initial winter warming at that height. This is the strong signature of the so-called mid-latitude mesospheric temperature inversions. Above TMF the mesospheric temperature inversions appear to occur 1 to 2 months later than above OHP and CEL as a consequence of the latitudinal variability. At this date, it is still not clear whether the winter mid-latitude temperature inversions around 70 km have the same origin as that of the equinoctial low-latitude inversions observed around 80 km by SME [13], ISAMS and HALOE [17], and by lidar at MLO.

The chaotic nature of the seasonal variations of the middle atmospheric temperature allows most of the discrepancies observed between the different measurement sites, or between the lidar and CIRA-86 climatologies, to be explained. Above TMF, the large positive departure from CIRA-86 in February is due to the second winter warming where the occurrence of the mesospheric temperature inversions has its maximum. The positive departure at 60 km in April and 60-70 km in late fall are related respectively to the late winter warming (February-March) and to the first winter warming (October). The negative maximum at 75-80 km is related to the stationary period trapped in October between the first and second winter warmings. Above MLO, it is more likely that most of the observed departure in the middle and upper mesosphere is related to tidal effects and/or the mesopause thermal SAO. The amplitudes of 1-5 K predicted by tidal models [7] is believed to be underestimated.

The climatology presented in this paper was obtained using composite temperature profiles from several years of measurements. Of course, a non-negligible interannual variability may disturb the temperature field from year to year. However, the trends already observed in previous climatologies [6] remain small compared to the seasonal variations. Also, the effect of volcanic eruptions, such Pinatubo in 1991 [19] and more recently Soufrière on Montserrat, may have non-negligible

disturbing effects. All trends, 11-year solar cycle, Quasi Biennial Oscillation (QBO), and volcanic eruption effects are currently being investigated. The use of such a complete climatology is crucial for many purposes such as providing a reference atmosphere for models and instruments, a background atmosphere for smaller scales studies, an overall comprehension of the strongly coupled lower-middle-upper atmosphere, and more. Until now, only a few instruments can provide such long-term data series. With the recent and future development of many ground-based lidars within the NDSC at many latitudes, a more complete climatology of the middle atmospheric temperature should be available within few years.

ACKNOWLEDGEMENTS

The work described in this paper was carried out, in part, at the Jet Propulsion Laboratory, California Institute of Technology, under an agreement with the National Aeronautics and Space Administration. TL thanks the National Research Council for the award of an associateship. The work at Colorado State University was supported by the National Science Foundation CEDAR program under ATM 91-01842 and ATM 94-15853. The long-term measurements at OHP and CEL have been supported by DRET, CNES and INSU for CNRS.

REFERENCES

1. A. Hauchecorne and M. L. Chanin, "Density and temperature profiles obtained by lidar between 35 and 70 km", *Geophys. Res. Lett.*, **7**, pp. 565-568, 1980
2. P. Keckhut, A. Hauchecorne, and M. L. Chanin, "A critical review of the database acquired for the long-term surveillance of the middle atmosphere by French Rayleigh lidars", *J. Atmos. Oceanic Technol.*, **10**, pp. 850-867, 1993
3. T. Leblanc, I. S. McDermid, A. Hauchecorne, and P. Keckhut, "Evaluation and optimization of lidar temperature analysis algorithms using simulated data", *J. Geophys. Res.*, **103**, pp. 6177-6187, 1998.
4. C. Y. She, J. R. Yu, H. Latifi, and R. E. Bills, "High-spectral-resolution fluorescence light detection and ranging for mesospheric sodium temperature measurements", *Appl. Opt.*, **31**, pp. 2095-2106, 1992.
5. I. S. McDermid, T. D. Walsh, A. Deslis and M. L. "White, Optical systems design for a stratospheric lidar system", *Appl. Opt..*, **34**, pp. 6201-6210, 1995.
6. A. Hauchecorne, M. L. Chanin, and P. Keckhut, "Climatology and trends of the middle atmospheric temperature (33-87 km) as seen by Rayleigh lidar over the south of France", *J. Geophys. Res.*, **96**, pp. 15,297-15,309, 1991.
7. M. E. Hagan, J. M. Forbes and F. Vial, "On modeling migrating solar tides", *Geophys. Res. Lett.*, **22**, pp. 893-896, 1995.
8. J. R. Yu, and C. Y. She, "Climatology of a midlatitude mesopause region observed by a lidar at Fort Collins, Colorado (40.6°N, 105°W)", *J. Geophys. Res.*, **100**, pp. 7441-7452, 1995.
9. D. C. Senft, G. C. Papen, C. S. Gardner, J. R. Yu, D. A. Krueger, and C. Y. She, "Seasonal variations of the thermal structure of the mesopause region at Urbana, IL (40°N, 88°W) and Ft. Collins CO (41°N, 105°W)", *Geophys. Res. Lett.*, **21**, pp. 821-824, 1994
10. F. J. Lubken, and U. Von Zahn, "Thermal structure of the mesopause region at polar latitudes", *J. Geophys. Res.*, **96**, pp. 20,841-20857, 1991.
11. R. E. Bills, and C. S. Gardner, "Lidar observations of the mesopause region temperature structure at Urbana", *J. Geophys. Res.*, **98**, pp. 1011-1021, 1993.
12. E. L. Fleming, S. Chandra, J. J. Barnett and M. Corney, "COSPAR International Reference Atmosphere, Chapter 2: Zonal mean temperature, pressure, zonal wind and geopotential height as functions of latitude", *Adv. Space Res.*, **10 (12)**, pp. 11-59, 1990.
13. R. T. Clancy, D. W. Rush, and M. T. Callan, "Temperature minima in the average thermal structure of the middle atmosphere (70-80 km) from analysis of 40- to 92-km SME global temperature profiles", *J. Geophys. Res.*, **99**, pp. 19,001-19,020, 1994.
14. R. R., Garcia, and R. T. Clancy, "Seasonal Variation in equatorial mesospheric temperatures observed by SME", *J. Atmos. Sci.*, **47**, pp. 1666-1673, 1990.
15. R. R. Garcia, T. J. Dunkerton, R. S. Lieberman, and R. A. Vincent, "Climatology of the semiannual oscillation of the tropical middle atmosphere", *J. Geophys. Res.*, **102**, pp. 26,019-26,032, 1997.
16. C. Y. She, J. R. Yu, D. A. Krueger, R. Roble, P. Keckhut, A. Hauchecorne, and M. L. Chanin, "Vertical structure of the midlatitude temperature from stratosphere to mesopause (30 - 105 km)", *Geophys. Res., Lett.*, **22**, pp. 377-380, 1995.
17. T. Leblanc, and A. Hauchecorne, "Recent observations of the mesospheric temperature inversions", *J. Geophys. Res.*, **102**, pp. 19,471-19,482, 1997.
18. B. N. Lawrence, and W. J. Randel, "Variability in the mesosphere observed by the Nimbus 6 pressure modulator radiometer", *J. Geophys. Res.*, **101**, pp. 23,475-23,489, 1996.
19. P. Keckhut, A. Hauchecorne, and M. L. Chanin, "Midlatitude long-term variability of the middle atmosphere: Trends and cyclic and episodic changes", *J. Geophys. Res.*, **100**, pp. 18,887-18,897, 1995.